COMMUNICATIONS IN COMPUTATIONAL PHYSICS
Vol. **1**, No. 2, pp. 336-361

Commun. Comput. Phys.
April 2006

Direct Numerical Simulation of Vertical Rotating Turbulent Open-Channel Flow with Heat Transfer

Bu-Yang Li[1], Nan-Sheng Liu[1] and Xi-Yun Lu[1,*]

[1] *Department of Modern Mechanics, University of Science and Technology of China, Hefei, Anhui 230026, P. R. China.*

Received 19 September 2005; Accepted (in revised version) 1 December 2005

Communicated by B. C. Khoo

Abstract. Direct numerical simulation of vertical rotating open-channel flow with heat transfer has been carried out for the rotation number N_τ from 0 to 0.1, the Prandtl number 1, and the Reynolds number 180 based on the friction velocity of non-rotating flow and the height of the channel. The objective of this study is to reveal the effect of rotation on the characteristics of turbulent flow and heat transfer, in particular near the free surface and the wall of the open-channel. Statistical quantities, e.g., the mean velocity, temperature and their fluctuations, turbulent heat fluxes, and turbulence structures, are analyzed. The depth of surface-influenced layer decreases with the increase of the rotation rate. In the free surface-influenced layer, the turbulence and thermal statistics are suppressed due to the effect of rotation. In the wall-influenced region, two typical rotation regimes are identified. In the weak rotation regime with $0 < N_\tau < 0.06$ approximately, the turbulence and thermal statistics correlated with the spanwise velocity fluctuation are enhanced since the shear rate of spanwise mean flow induced by Coriolis force increases; however, the other statistics are suppressed. In the strong rotation regime with $N\tau > 0.06$, the turbulence and thermal statistics are suppressed significantly because the Coriolis force effect plays a dominant role in the rotating flow. To elucidate the effect of rotation on turbulent flow and heat transfer, the budget terms in the transport equations of Reynolds stresses and turbulent heat fluxes are investigated. Remarkable change of the direction of streak structures based on the velocity and temperature fluctuations is discussed.

Key words: Direct numerical simulation (DNS); rotating turbulent flow; turbulent heat transfer; thermal statistics; coherent structure.

*Correspondence to: Xi-Yun Lu, Department of Modern Mechanics, University of Science and Technology of China, Hefei, Anhui 230026, P. R. China. Email: xlu@ustc.edu.cn

1 Introduction

Turbulent flows with heat transfer in a rotating frame exist in a variety of industrial, geophysical, and astrophysical applications. The rotation induces additional body forces, i.e., centrifugal and Coriolis forces, acting on the turbulent flow, so that the momentum transfer mechanism becomes more complex. Understanding the mechanism of turbulent flow and heat transfer in rotating system is of great importance. Usually, a simple and convenient way to investigate rotating turbulent flow is rotating channel flows, where the rotating axis can be chosen as that parallel to one of the three directions, i.e., the streamwise, spanwise and wall-normal directions [1].

The spanwise rotating turbulent channel flows have been studied experimentally and numerically [2-7]. With increasing rotation rate, turbulence is gradually enhanced on the pressure side and reduced on the suction side. Large-scale rotational-induced roll cells due to Taylor-Görtler instability occur in the cross-sectional plane of the channel [2, 3]. On the other hand, the streamwise rotating turbulent channel flows were also investigated numerically. Compared with the spanwise rotation effect, the influence of the streamwise rotation on turbulent channel flow is much weaker [1]. The streamwise rotation induces a mean velocity in the spanwise direction. The quasi-streamwise near-wall vortical structures rotating in the same direction are enhanced, whereas the opposite ones are reduced, and consequently the average spacing between the low- and high-speed streaky structures becomes much larger than that in a non-rotating channel flow.

In a wall-normal rotating channel flow, since the mean vorticity component is perpendicular to the rotating axis, turbulent channel flow is very sensitive to the wall-normal rotation, even though a slight system rotation can induce a significant spanwise mean velocity [1]. As a result, the absolute mean flow deviates from the initial streamwise direction, which redirects the mean shear and the turbulence structures. The interaction between the vorticity of coherent structures and the background vorticity due to imposed wall-normal rotation can significantly change the near-wall turbulence behavior [8, 9]. The statistical coherent structures are verified to be more sensitive to the Coriolis force effect induced by the wall-normal rotation.

It is well established that direct numerical simulation (DNS) is effective to explore the mechanism of turbulent flow and heat transfer and to provide detailed turbulence and thermal quantities which are essential to construct a turbulence model [7, 10, 11]. The determination of the thermal budget terms in the transport equations of turbulent heat fluxes is of great importance to the closure of the turbulent heat fluxes. Based on the DNS of turbulent channel flow with heat transfer, it is found that the temperature-pressure gradient correlation is a dominant term in the budget of wall-normal turbulent heat flux [12, 13]. The turbulent diffusion and dissipation terms in the budgets of turbulent heat fluxes are physically meaningful to the construction and assessment of the turbulence model involving heat transfer [7, 11]. Thus, it is highly tempting to investigate the effects of rotation on the budget terms of turbulent heat fluxes.

As described above, extensive investigations of the rotating two-walled channel flows

have been carried out, with focus mainly on the turbulence statistics and near-wall structures. To the best of our knowledge, however, little work on the vertical rotating open-channel flow with heat transfer has been undertaken. In this study, direct numerical simulations of the vertical rotating turbulent open-channel flows with heat transfer are performed to study the characteristics of turbulent flow and heat transfer, in particular, near the wall and the free surface.

This paper is organized as follows. The mathematical formulation is described in Section 2. The numerical method is given in Section 3. In Section 4, statistical turbulence and heat transfer quantities, the budget terms in the transport equations of Reynolds stresses and turbulent heat fluxes, and the structures near the wall and the free surface are discussed. Finally, concluding remarks are summarized in Section 5.

2 Mathematical formulation

The incompressible Navier-Stokes and energy equations are used for direct simulation of fully developed turbulent flow with heat transfer in a vertical rotating open-channel, as shown in Fig. 1 for the sketch. To normalize the governing equations, the wall friction velocity u_τ of non-rotating channel flow is used as the velocity scale, the height of the channel h as the length scale, and the temperature difference ΔT between the free surface and the bottom wall as the temperature scale. The non-dimensional governing equations are thus given as

$$\frac{\partial u_i}{\partial x_i} = 0 \tag{2.1}$$

$$\frac{\partial u_i}{\partial t} + \frac{\partial u_i u_j}{\partial x_j} = -\frac{\partial p}{\partial x_i} + \delta_{1i} + \frac{1}{Re_\tau}\frac{\partial^2 u_i}{\partial x_j \partial x_j} - N_\tau \varepsilon_{ijk}\frac{\Omega_j}{|\Omega|}u_k \tag{2.2}$$

$$\frac{\partial T}{\partial t} + \frac{\partial (T\, u_j)}{\partial x_j} = \frac{1}{Re_\tau \,\mathrm{Pr}}\frac{\partial^2 T}{\partial x_j \partial x_j} \tag{2.3}$$

where p represents the effective pressure combined with the centrifugal force. The non-dimensional parameters in this problem are the rotation, Reynolds and Prandtl numbers, which are defined as $N_\tau = 2|\Omega|h/u_\tau$, $Re_\tau = u_\tau h/\nu$ and $\mathrm{Pr} = \nu/\kappa$, respectively, with Ω being the angular speed of rotating frame, ν the kinematic viscosity, and κ the thermal diffusivity.

At the wall $y = 0$, no-slip velocity condition is imposed. Assuming the free surface being in the absence of significant surface deformation, the boundary conditions applied at $y = 1$, for a shear free interface without deformation, are given as

$$v = 0, \quad \frac{\partial u}{\partial y} = \frac{\partial w}{\partial y} = 0. \tag{2.4}$$

The flow and temperature fields are assumed to be statistically homogeneous in the streamwise and spanwise directions. Thus, periodic boundary conditions are employed in both

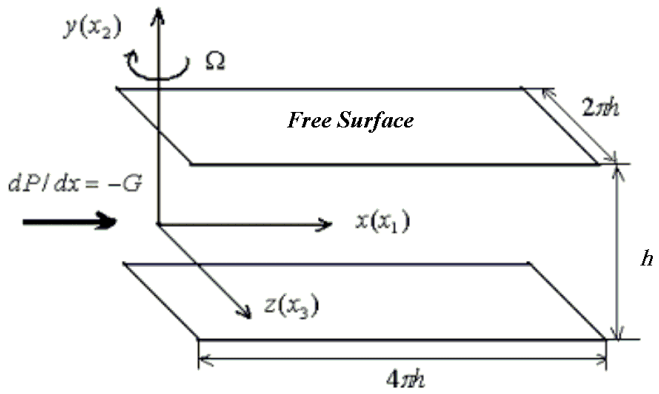

Figure 1: Sketch of the vertical rotating open-channel flow with heat transfer.

the directions. Two different constant temperatures, i.e., $T_F = 0.5$ and $T_W = -0.5$, are imposed on the free surface and the wall, respectively. Heat transfer computation is started after the flow field has statistically reached a fully developed turbulent state. Initial temperature field is set to be a linear distribution along the vertical direction and homogeneous in the horizontal plane.

3 Numerical methods

To solve Eqs. (2.1)-(2.3), a fractional-step method developed by Verzicco and Orlandi [14] is used. Spatial derivatives are discretized by a second-order central difference. Time advancement is carried out by the semi-implicit scheme using the Crank-Nicolson scheme for the viscous terms and the three-stage Runge-Kutta scheme for the convective terms. The discretized formulation was described in detail by Verzicco and Orlandi [14]. This method simplifies the boundary condition of the non-solenoidal velocity field, while retaining the feature of the algorithm developed by Kim and Moin [15] and Rain and Moin [16], and has the additional advantage that the minimum amount of computer run-time memory is realized.

In this study, the mesh number is 193×193×193 with the corresponding computational domain $4\pi h \times h \times 2\pi h$ in the streamwise, vertical, and spanwise directions, respectively. This grid system is fine enough to resolve all essential scales of the low-Reynolds-number turbulence and contains the largest scale structures in the channel [17]. A stretching transformation is employed to obtain fine grid resolution near the wall and the free surface. The grid point close to the boundary is located at $y^+ = 0.3$ approximately, while the largest spacing is about $\Delta y^+ = 4.5$ in the center of the channel, where y^+ is defined as $y^+ = (1 - |y/h|)Re_\tau$. Uniform grids are employed in both the streamwise and spanwise directions with the grid spacing $\Delta x^+ = 12.6$ and $\Delta z^+ = 9.5$, respectively. To ensure the computational domain size being enough, two-point correlations in the streamwise and

spanwise directions have been calculated to be negligibly small values, indicating that the computational domain used is large enough.

It is worthwhile to mention that the performance and reliability of the numerical method and the relevant code employed here have been verified based on the DNS of rotating and non-rotating turbulent pipe flows [18-20]. Furthermore, the finite difference schemes with the second-order accuracy are widely used in the DNS of turbulent and transitional flows, e.g., rotating channel flow [3, 21], annular pipe flow [22], oscillatory flow in the boundary layer and pipe [23, 24], and turbulent Rayleigh–Bénard convection flow [25]. It was confirmed that the numerical method with the second-order accuracy schemes succeeded in predicting the turbulence characteristics.

The relevant method and code used in this study have been verified in our previous work [8, 26-33]. To validate the present DNS, as exhibited in [8, 33], our calculated results are in good agreement with previous DNS results. It can be ensured that the numerical method is reliable to predict the turbulence characteristics for the vertical rotating open-channel flows.

4 Results and discussion

4.1 Turbulence statistics

The profiles of the mean velocity in the streamwise and spanwise directions are shown in Figs. 2(a) and 2(b). When the vertical rotation is imposed, the streamwise mean velocity $< u >$ decreases monotonically with the increase of N_τ, indicating the reduction of the wall shear rate related to the streamwise mean flow. In Fig. 2(b), the spanwise mean velocity $< w >$ increases as N_τ varies from 0 to 0.06; however, as N_τ increases further, e.g., at $N_\tau = 0.08$ and 0.1, the spanwise mean flow is suppressed obviously, due to the Coriolis force induced by the rotation.

Distributions of the turbulence intensities, i.e., the root-mean-square (rms) values of the streamwise, vertical, and spanwise velocity fluctuations, are shown in Fig. 3. In pure shear channel flow, only the streamwise mean velocity exists. The streamwise velocity fluctuation is mainly generated by the shear process of the streamwise mean flow, while the mechanism to generate the spanwise velocity fluctuation is the splattering effect induced by the high-speed streaky structures rushing to the wall and the low-speed ones lifting from the wall [34]. However, in the vertical rotating channel flow, since the Coriolis force induces the spanwise mean velocity shown in Fig. 2b, there exist both the streamwise and spanwise mean shear effects. Thus, the production of the streamwise velocity fluctuation comes from both processes. One is the shear process related to $< u >$, which is an important source to generate the streamwise velocity fluctuation in weakly rotating case, and the other the splattering effect associated with $< w >$. Similarly, the shear process of the spanwise mean flow takes a major responsibility to generate the spanwise velocity fluctuation in strong rotation flow. Correspondingly, turbulent heat transfer in the spanwise direction is also induced significantly due to the spanwise mean flow and will be discussed in the following

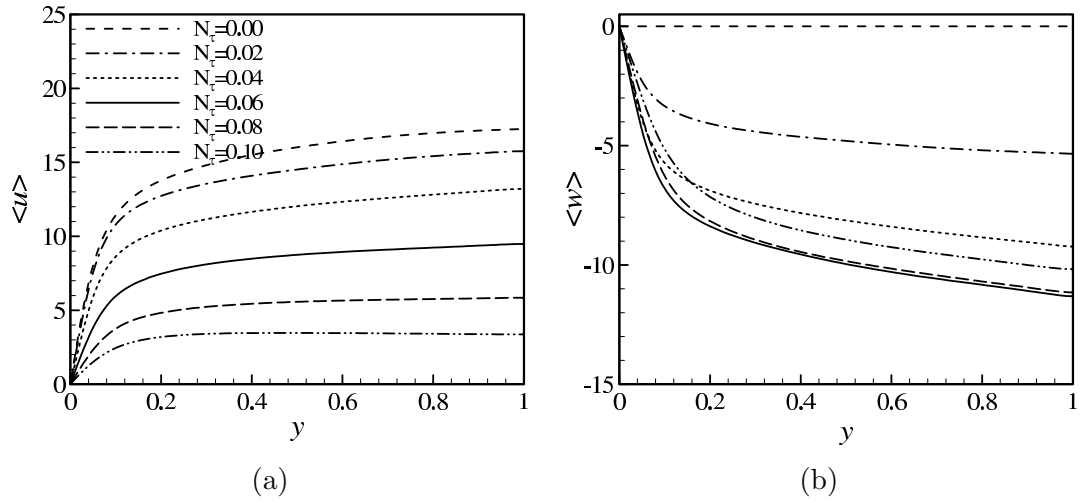

Figure 2: Profiles of the mean velocities: (a) streamwise component; (b) spanwise component.

subsection.

In the wall-influenced region, as N_τ increases, the near-wall shear rate related to $<u>$ reduces significantly. Thus, a rapid drop of the streamwise velocity fluctuation u'_{rms} is observed in Fig. 3(a). Similarly, the vertical velocity fluctuation v'_{rms} in Fig. 3(b) decreases. As shown in Fig. 3(c), when N_τ varies from 0 to 0.06, the spanwise velocity fluctuation w'_{rms} is enhanced remarkably due to increasing the spanwise mean shear rate, as shown in Fig. 2(b). The high near-wall peak value of w'_{rms} at $N_\tau = 0.06$, compared with other rotating cases, is attributed to strong shear rate of the spanwise mean flow. When the rotation rate increases further, e.g., $N_\tau = 0.08$ and 0.1, the mechanism for turbulence fluctuation generation is suppressed apparently by the Coriolis force effect, which causes the reduction of all three turbulence intensities.

Here, we further discuss turbulence characteristics in the free surface-influenced layer, which have never been studied for the vertical rotating turbulent open-channel flow. The depth of the surface-influenced region can be qualitatively denoted by the position where the free surface begins to damp the vertical velocity fluctuation v'_{rms} [35], correspondingly, to enhance the spanwise velocity fluctuation w'_{rms} because the turbulence energy is mainly transferred from the vertical to spanwise direction near the free surface due to the organized structure represented as "dipole vorticity" along the streamwise direction [29]. In the rotating flow, the organized structures near the free surface redirect to the spanwise from the streamwise direction due to the effect of rotation. The spanwise velocity fluctuation in Fig. 3 is mainly obtained from the vertical velocity fluctuation near the free surface and may be used to identify qualitatively the surface-influenced region. From Fig. 3(d) for the profiles of w'_{rms} near the free surface, the depth of the surface-influenced region (y_D^+), which is normalized by wall parameters, can be determined approximately by the distance from the free surface to the location of minimum of w'_{rms} [35, 36] and is shown in

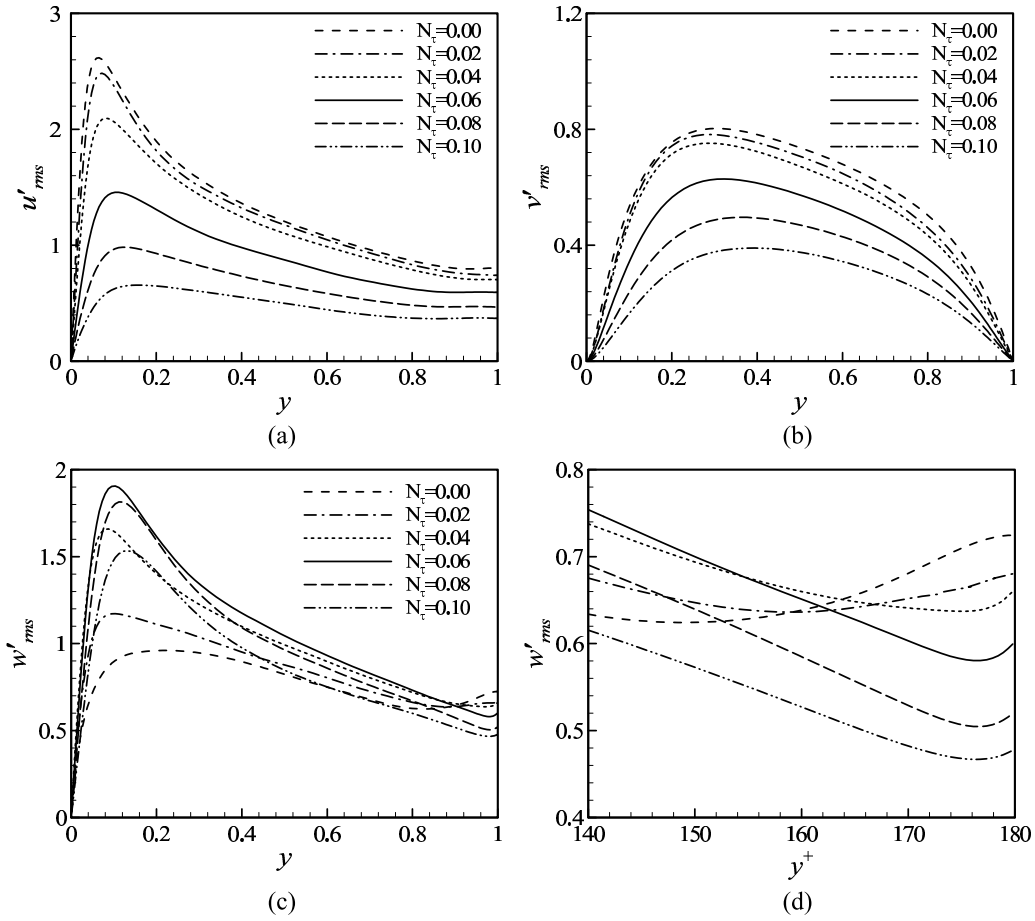

Figure 3: Turbulence intensities: (a) streamwise; (b) vertical; (c) spanwise; (d) spanwise intensity near the free surface.

Fig. 4. It is reasonably predicted that the depth of the surface-influenced layer decreases with the increase of the rotation rate and, as shown in Fig. 3, the turbulence intensities in the free surface-influenced layer are suppressed.

The effect of the vertical rotation on the turbulent flow is obvious to change the absolute mean flow direction, i.e., tilting to the spanwise direction. Thus, the elongated near-wall streaky structures generated by the shear process of the absolute mean flow are expected to deviate from the streamwise to the spanwise direction. This suggests that the high-speed (relative to the absolute mean flow) near-wall streaks, corresponding to the sweep events [17, 37], are related to the fluid with velocity fluctuations $u' > 0$, $w' < 0$ and $v' < 0$ in the rotating flow, while the low-speed streaks responsible for the ejection events correspond to $u' < 0$, $w' > 0$ and $v' > 0$. These relations between the velocity fluctuations are helpful to determine the sign of cross Reynolds stresses in the wall region.

Fig. 5 shows the profiles of the cross Reynolds stresses. The cross Reynolds stresses

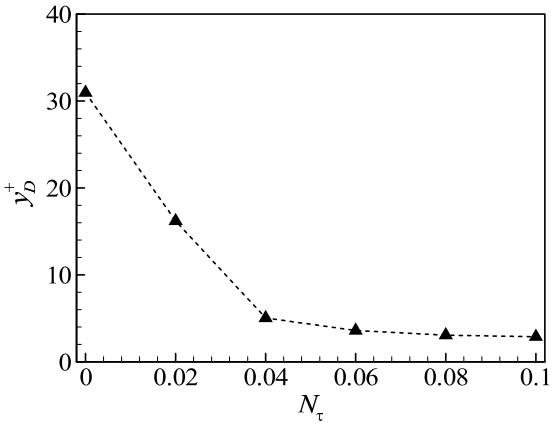

Figure 4: Depth of the surface-influenced region normalized by wall parameters.

$<u'v'>$ and $<u'w'>$ are found to be negative in the wall region, while the cross Reynolds stress $< v'w' >$ to be positive, which is consistent with the above description for the ejection and sweep events. The $< u'v' >$ is mainly related to the change of $< u >$ and subsequently decreases with the increase of N_τ. In weak rotation, e.g., $N_\tau = 0.02$, a slight alteration of the cross Reynolds stress occurs. However, in strong rotation, e.g., N_τ =0.1, the $<u'v'>$ becomes nearly zero over the channel, indicating a poor correlation between the streamwise and vertical velocity fluctuations. The distribution of $< u'v' >$ contains a noticeable linear region when $y > 0.3$ approximately, and the $< v'w' >$ also shows a linear distribution there in the rotating cases. These behaviors of $<u'v'>$ and $<v'w'>$ should be ascribed to the co-existence of the streamwise and spanwise mean flows in the rotating flow. The $< v'w' >$, which is related to the change of $< w >$, is enhanced as N_τ varies from 0 to 0.06 and suppressed as N_τ from 0.06 to 0.1. As shown in Fig. 5(c) for the distributions of $<u'w'>$, similar behavior versus N_τ is observed. The near-wall alterations of $<v'w'>$ and $<u'w'>$ are attributed to the shear rate of the spanwise mean flow, because $\partial < w > /\partial y$ contributes directly to the production rate of both the cross Reynolds stresses based on the analysis of the transport equation of Reynolds stresses.

4.2 Temperature and thermal statistics

Further, the effect of rotation on turbulent heat transfer is discussed. The profiles of the mean temperature are shown in Figs. 6(a) and 6(b). Unlike the two-walled channel flow [38], the profiles in Fig. 6(a) in global coordinate do not exhibit the anti-symmetry with respect to the central line (i.e., $y = 0.5$) of the open-channel. To clearly exhibit the distributions of the temperature near the wall, as shown in Fig. 6(b), where $<T^+>$ is defined as

$$< T^+ >= [< T > -T_W]/T_\tau, \tag{4.1}$$

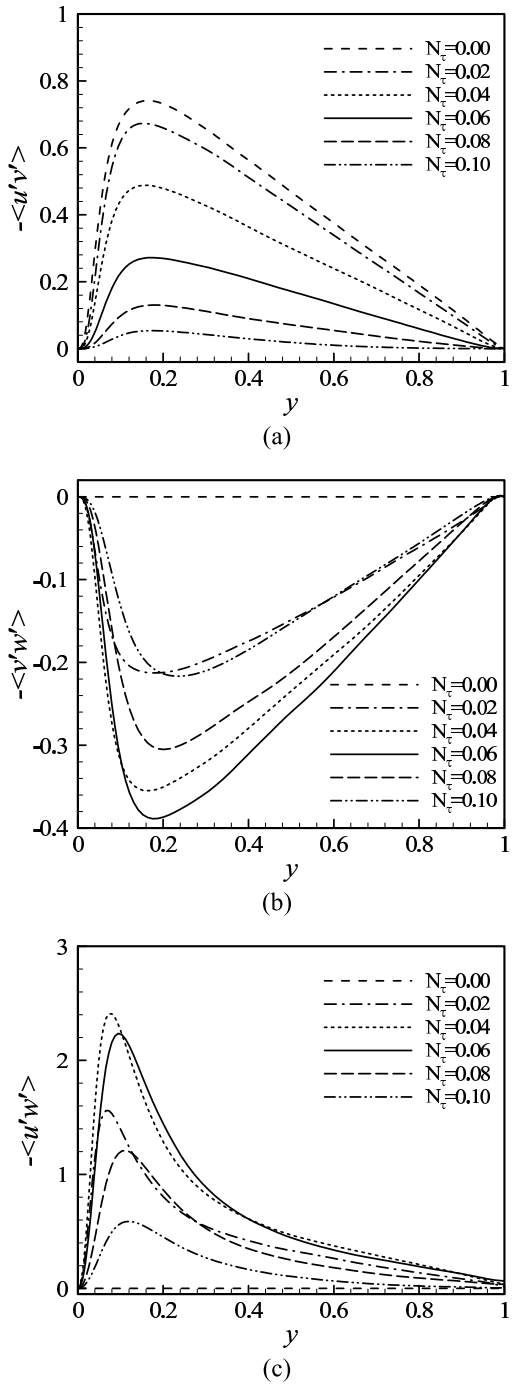

Figure 5: Profiles of the shear stresses: (a)$<u'v'>$ (b)$<v'w'>$ (c)$<u'w'>$.

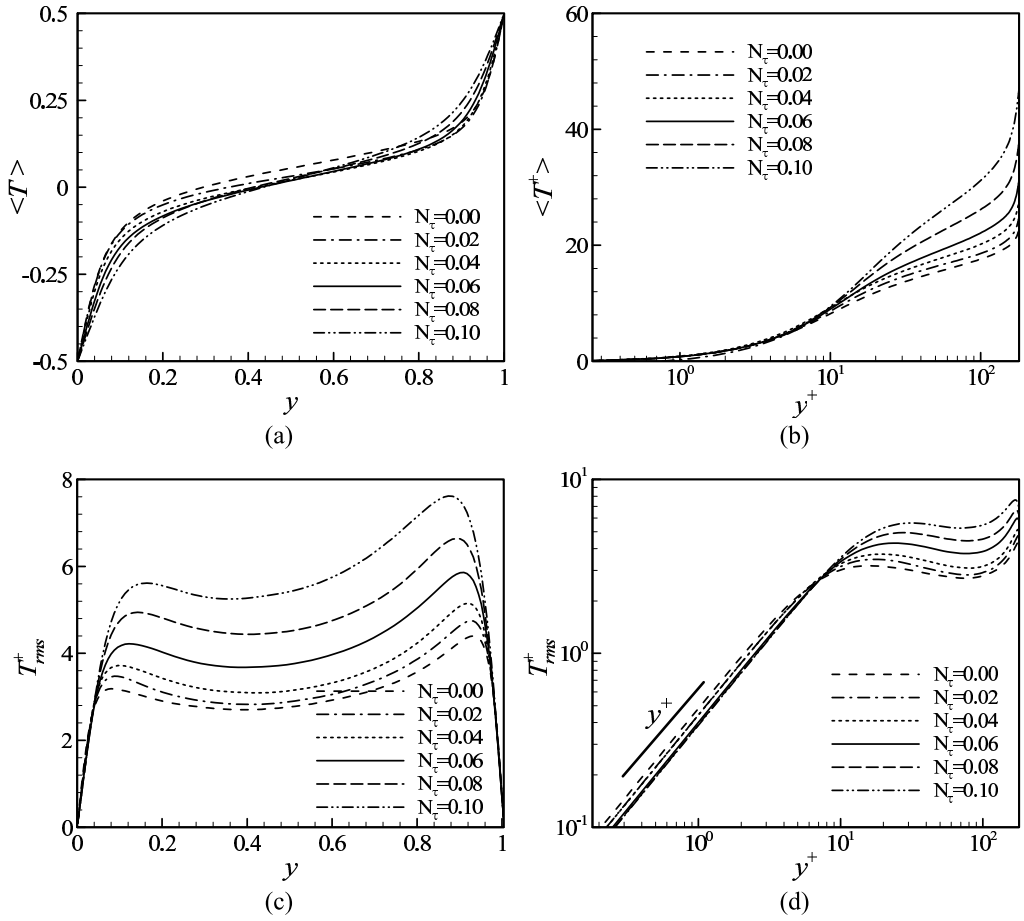

Figure 6: Temperature statistics: (a) mean temperature over the channel; (b) mean temperature near the wall; (c) temperature fluctuation over the channel; (d) temperature fluctuation near the wall.

where T_τ is the friction temperature and is obtained by

$$T_\tau = \frac{\kappa}{u_\tau}\left|\frac{d<T>}{dy}\right|_{y=0}. \tag{4.2}$$

Similar to the mean velocity distribution in Fig. 2, there exists a buffer layer followed by a logarithmic region in the mean temperature profile. It is noticed that, based on the profiles near the wall in Fig. 6(a), the friction temperature decreases with the increase of N_τ.

Figs. 6(c) and 6(d) show the profiles of the temperature fluctuation, normalized by the friction temperature. With increasing N_τ, the peak values of temperature fluctuations near the wall and the free surface increase and their positions shift away from the wall and the free surface. Note that, when the distance from the wall goes to zero, as exhibited in Fig. 6(d) by the curve of the linear law with y^+, the temperature fluctuations approach

zero linearly with a slope that is almost independent of N_τ. As similar behavior is also found near the free surface.

The Nusselt number is an important parameter relevant to the heat transfer coefficient and is defined, at the free surface, by

$$Nu = \frac{q_F h}{k\Delta T}, \tag{4.3}$$

where q_F represents the averaged heat flux through the free surface, and k is the thermal conductivity. In the case of purely diffusive heat transport through a stationary fluid, Nu=1; thus the value of Nu quantifies the increases of heat transport across a free surface due to turbulence with respect to its laminar value. From the mean temperature profiles in Fig. 6(a), Nu is obtained and is shown in Fig. 7. It is found that a linear relationship between Nu and N_τ occurs approximately for the range of N_τ considered here. As turbulence is suppressed globally with the increase of N_τ, it is reasonably predicted that Nu decreases. Komori et al. [39] and Rashidi et al. [40] investigated the passive heat transfer at the free surface for the non-rotating case and obtained a general relationship between the Reynolds number and the Nusselt number. At Ri_τ =0, our calculated data $Nu = 5.7$ agrees well with $Nu = 5.6$ [39] and 6.0 [40].

Furthermore, there is fairly recent experimental work by Law and Khoo [41] where an empirical relationship is obtained between the scalar transport across the interface and the turbulence statistics expressed in terms of the gradient of the vertical fluctuating velocity at the interface. Then, by a non-dimensional analysis, the empirical relationship is expressed as

$$Nu\mathrm{Pr}^{0.5} = 0.22\left(Re_\tau \left|\frac{\partial v'_{rms}}{\partial y}\right|_{y=1}\right)^{0.5}. \tag{4.4}$$

As shown in Fig. 7, the data predicted by (4.4) and the present DNS agree quite well with each other. Since the empirical relation is obtained independent of the means of turbulence generation close to the interface [41], it is thus applicable in the presence of a rotating field with $N_\tau \neq 0$. The good comparison represents that the relationship is more applicable for engineering purposes and supports the findings of the motion of universality of the small-eddy model used to account for the physics of interfacial scalar transfer [41].

Since a fully developed turbulent flow is assumed, the statistical thermal equilibrium is achieved with a relationship [12, 31],

$$\frac{1}{Re_\tau \,\mathrm{Pr}} < \frac{\partial T^+}{\partial y} > - < T'^+ v' >= 1. \tag{4.5}$$

The first term on the left-hand side represents the heat flux relevant to the molecular thermal diffusion, and the second one is the vertical turbulent heat flux. Thus, Eq. (4.5) represents the fact that the total heat flux across the channel is the sum of the molecular and the vertical turbulent heat flux. To specify the portions of both the terms in (4.5),

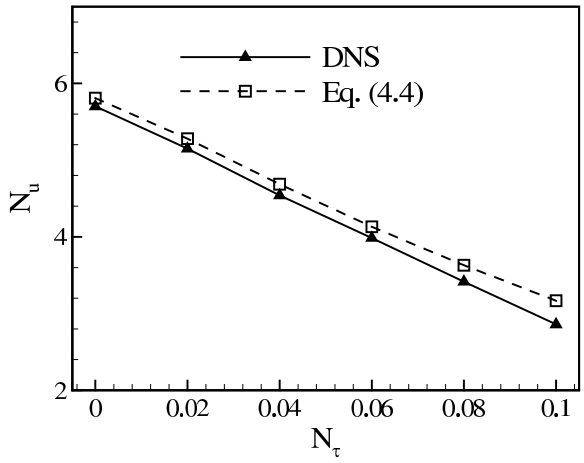

Figure 7: Profile of the Nusselt number and the comparison with the data predicted by (4.4).

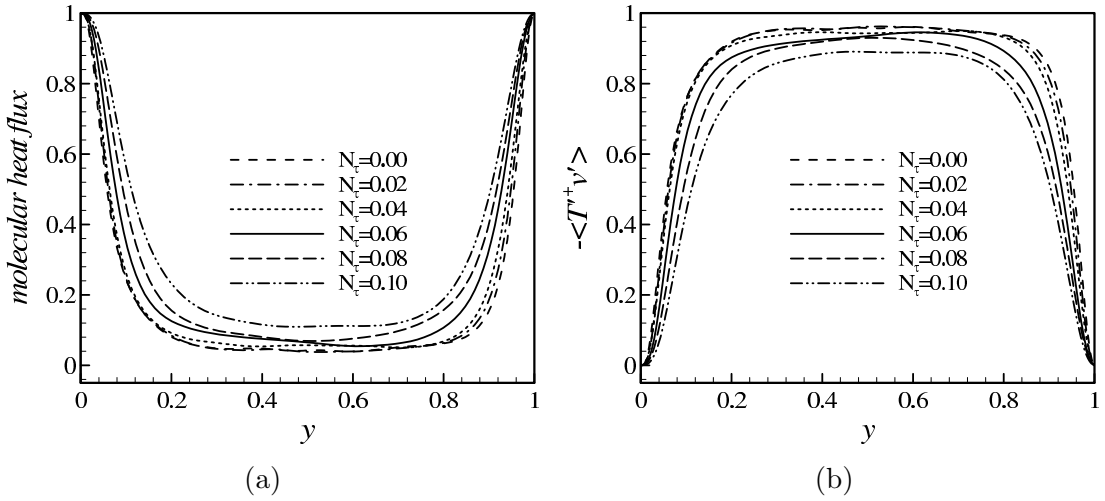

Figure 8: Distributions of the vertical heat flux: (a) molecular heat flux; (b) turbulent vertical heat flux.

the profiles are shown in Fig. 8. It is confirmed that our calculated results in Fig. 8 agree well with (4.5). This behavior also ensures that the temperature field is fully developed and the present calculation is accurately reliable.

As shown in Fig. 8, in the regions of the wall and the free surface, the vertical turbulent heat flux ($-<T'^+v'>$) reduces as N_τ increases, while the contribution of the molecular diffusion to the total vertical heat flux increases correspondingly. This means that the molecular heat flux is enhanced due to the effect of rotation. In the core region, $-<T'^+v'>$ is somewhat below unity in Fig. 8(b); it is because, as shown in Fig. 6(a), the non-zero mean temperature gradient occurs. Thus, the vertical heat flux is mainly contributed by the molecular diffusion in the regions near the wall and the free surface and by the

turbulent motion in the core region of the channel.

Fig. 9 shows the profiles of the turbulent heat fluxes in the streamwise, vertical, and spanwise directions, respectively, where the temperature fluctuation is normalized by the friction temperature. As N_τ increases, the streamwise and vertical turbulent heat fluxes, i.e., $<T'^{+}u'>$ and $-<T'^{+}v'>$, in the near wall region, are reduced. It is noted that, the spanwise turbulent heat flux, i.e., $-<T'^{+}w'>$, is apparently enhanced when N_τ varies from 0.02 to 0.06, and suppressed when N_τ from 0.06 to 0.1. Since the turbulent heat fluxes are closely related to the velocity fluctuations, the features of turbulent heat fluxes versus N_τ are well consistent with the turbulence intensities in Fig. 3.

Considering the velocity and temperature boundary conditions, the turbulent heat fluxes can be expanded into power series of y^+ in the vicinity of the wall,

$$<T'^{+}u'> = a_1 y^{+^2} + a_2 y^{+^3} + ... \tag{4.6a}$$

$$<T'^{+}v'> = b_1 y^{+^3} + b_2 y^{+^4} + ... \tag{4.6b}$$

$$<T'^{+}w'> = c_1 y^{+^2} + c_2 y^{+^3} + ... \tag{4.6c}$$

Then, the curves of the square and cubic laws with y^+ are plotted in Fig. 9 with logarithmic scales to exhibit the first terms in (4.6). As expected, the turbulent heat fluxes agree well with the leading terms in (4.6) in the near wall region.

4.3 Turbulence budgets

The Reynolds stress budgets are helpful for the understanding of the rotation effect on dynamical characteristics of turbulence. From our calculated results, it is found that the behaviors of the Reynolds stress budgets are similar to those in the wall-normal rotating two-walled channel flows [8]. Here, we only examine the influence of the vertical rotation on the turbulence production rate, which can be represented as,

$$P_{ij} = -\left[<u_i'u_k'>\frac{\partial <u_j>}{\partial x_k} + <u_j'u_k'>\frac{\partial <u_i>}{\partial x_k}\right], \tag{4.7}$$

where repeated indices represent the summation over 1, 2, 3, corresponding to the streamwise, vertical, and spanwise directions, respectively.

Since there exist both the streamwise and spanwise mean velocities shown in Fig. 2, the corresponding turbulence production rates, i.e., P_{11} and P_{33}, are shown in Fig. 10, where the budget terms are re-scaled by u_τ^4/ν [42]. The positive production rate P_{11} assumes a major responsibility in the generation of the streamwise velocity fluctuation by the shear process of the streamwise mean flow [34], and contributes greatly to the $<u'u'>$ budget in the region around $y^+ = 10$ in Fig. 10(a). Since both the streamwise mean shear rate $\partial <u>/\partial y$ in Fig. 2(a) and the cross stress $-<u'v'>$ in Fig. 5(a) decrease, a remarkable reduction of P_{11} occurs in the rotating cases, indicating the decrease of the streamwise turbulence fluctuation. At $N_\tau = 0.1$, P_{11} even becomes negligibly small compared with

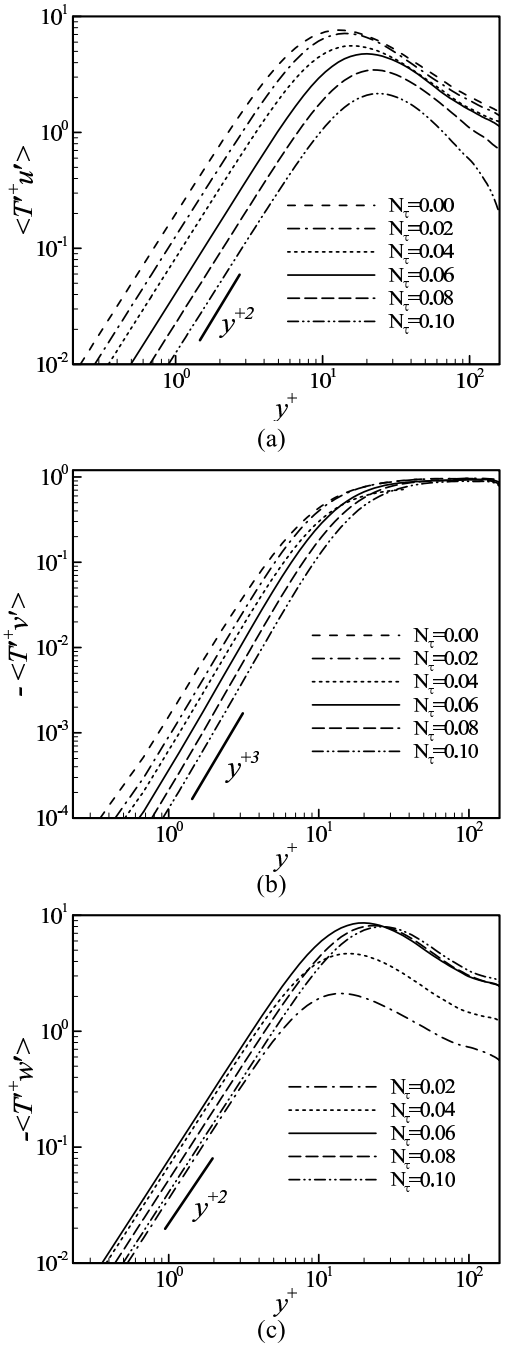

Figure 9: Distributions of the turbulent heat fluxes: (a) streamwise; (b) vertical; (c) spanwise.

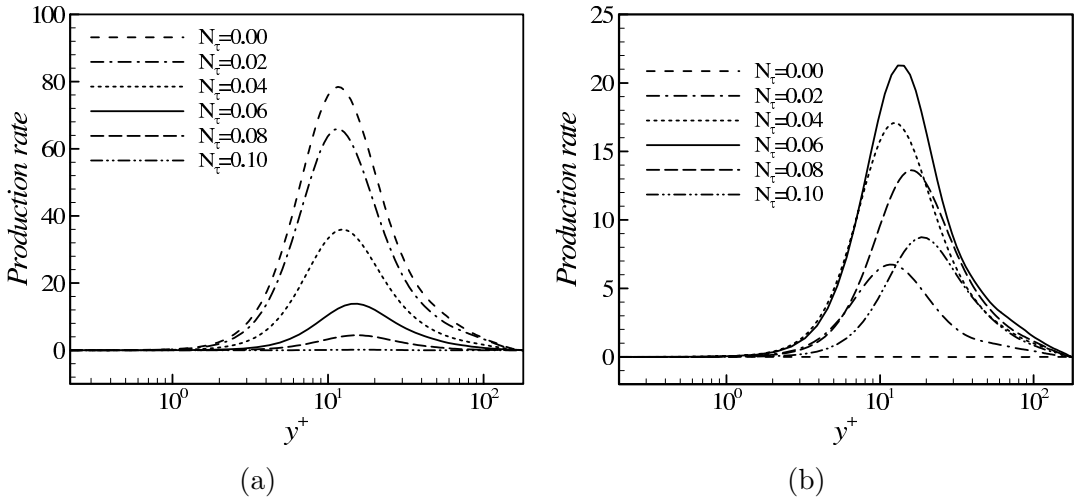

Figure 10: Distributions of the turbulence production rate: (a) streamwise; (b) spanwise.

the non-rotating flow. It is observed that the location of the peak value of P_{11} shifts away from the wall with increasing N_τ.

In the presence of the spanwise mean flow induced by the Coriolis force effect, the turbulence production rate in the spanwise direction occurs in Fig. 10(b). The production rate P_{33} is absent in pure shear channel flow (i.e., $N_\tau = 0$), and acts a main contribution to the generation of the spanwise velocity fluctuation around $y^+ = 10$ for the rotating flows. When N_τ increases to 0.06, P_{33} increases significantly; however, when N_τ increases from 0.06, P_{33} obviously decreases. This behavior is well consistent with the spanwise turbulence intensities in Fig. 3(c).

As shown in Fig. 3, the turbulence intensities have a strong anisotropy near the free surface. Analyses of the turbulence kinetic energy and dissipation budgets have revealed that anisotropic dissipation and pressure-strain effects are principally responsible for the anisotropy [29, 43]. Near the free surface, the dissipation becomes anisotropic due to the shear-free surface boundary conditions. Thus, the vertical fluctuation is preferentially dissipated, leading to an increase in stress anisotropy. To elucidate the mechanism of strong anisotropy subject to the effect of rotation, the characteristics of the pressure-strain on the energy transfer near the free surface are discussed here. The pressure-strain tensor is described as

$$\phi_{ij} =< p'(\frac{\partial u_i'}{\partial x_j} + \frac{\partial u_j'}{\partial x_i}) >, \tag{4.8}$$

where p' represents the pressure fluctuation. The trace of this tensor (ϕ_{ij}) is always zero because of the incompressiblility constraint. The distributions of the pressure-strain terms are shown in Fig. 11. Considering the profiles for the same N_τ, the value of the pressure-strain in the streamwise direction (ϕ_{11}) near the free surface is somewhat smaller than the value of the pressure-strain in the spanwise direction (ϕ_{33}), while ϕ_{33} increases in the

vicinity of the free surface and remains positive. The pressure-strain in the vertical direction (ϕ_{22}) decreases near the free surface and its sign changes from positive to negative. Thus, the turbulence energy in the vertical direction is mainly transferred into the spanwise direction through the pressure-strain effect and, as shown in Fig. 3(d), the turbulence intensity in the spanwise direction increases obviously near the free surface.

To exhibit the effect of rotation on the distributions of ϕ_{ii} ($i = 1, 2, 3$), as shown in Fig. 11, the absolute values of ϕ_{ii} near the free surface (or $y^+ > 170$ approximately) decrease with the increase of N_τ, and the turbulence intensities near the free surface shown in Fig. 3 are suppressed.

4.4 Thermal budgets

To explore the effect of rotation on the turbulent heat transfer, we analyze the budget terms in the transport equations of turbulent heat fluxes $<T'u_i'>$, which are given in the Appendix, by taking the ensemble average on Eqs. (2.2) and (2.3). Due to the inhomogeneity introduced by the wall and the free surface, the terms in the budgets have a strong dependence on the distance from the wall and the primary balance involves different terms at different heights.

All the budget terms in the streamwise turbulent heat flux $< T'u' >$ are shown in Fig. 12 for different rotation numbers. As a typical case, we first consider the budget balance at N_τ =0.06. In the thermal diffusive sublayer $y^+ < 3$, the budget is balanced mainly between MV_1 and DS_1. In the region around $y^+ = 15$, the terms of $< T'u' >$, i.e., PV_1, PT_1, TD_1, DS_1 and MV_1 terms, are mainly contributed to the budget balance and other terms are relatively small. Both PV_1 and PT_1 act as source terms to generate $<T'u'>$ over the channel, and MV_1 changes its sign from positive to negative at $y^+ = 6$ approximately. All the terms reduce gradually with the increase of y^+ outside the wall region. In the rotating flow, the non-zero Coriolis force term CO_1 arises, however, is negligibly small, compared to the other terms.

To exhibit the effects of rotation on the budget terms in $<T'u'>$, as shown in Fig. 12, with the increase of N_τ, the magnitudes of all the budget terms except the Coriolis force term CO_1 decrease monotonically. The term CO_1 increases with N_τ and is relatively small; it means that the Coriolis force has little influence on the budget balance of $<T'u'>$.

In the vertical rotating channel flow, there exist the spanwise mean velocity shown in Fig. 2b due to the Coriolis force and the spanwise turbulent heat flux in Fig. 9c. To reveal the mechanism related to the spanwise turbulent heat flux, the budget terms in the transport equation of spanwise turbulent heat flux, i.e., $< T'w' >$, are shown in Fig. 13. As a typical case for N_τ =0.06, in the thermal diffusive sublayer $y^+ < 3$, DS_3 acts as a dominate term and is balanced mainly with MV_3 and MT_3; this feature is different from the streamwise turbulent heat flux in Fig. 12. In the region around $y^+ = 15$, all the budget terms, except for CO_3 with negligibly small value, play as major contribution to the budget balance. In the region for $y^+ > 30$ approximately, all the budget terms decrease with y^+. To deal with the effect of rotation on the budget terms in $<T'w'>$, it

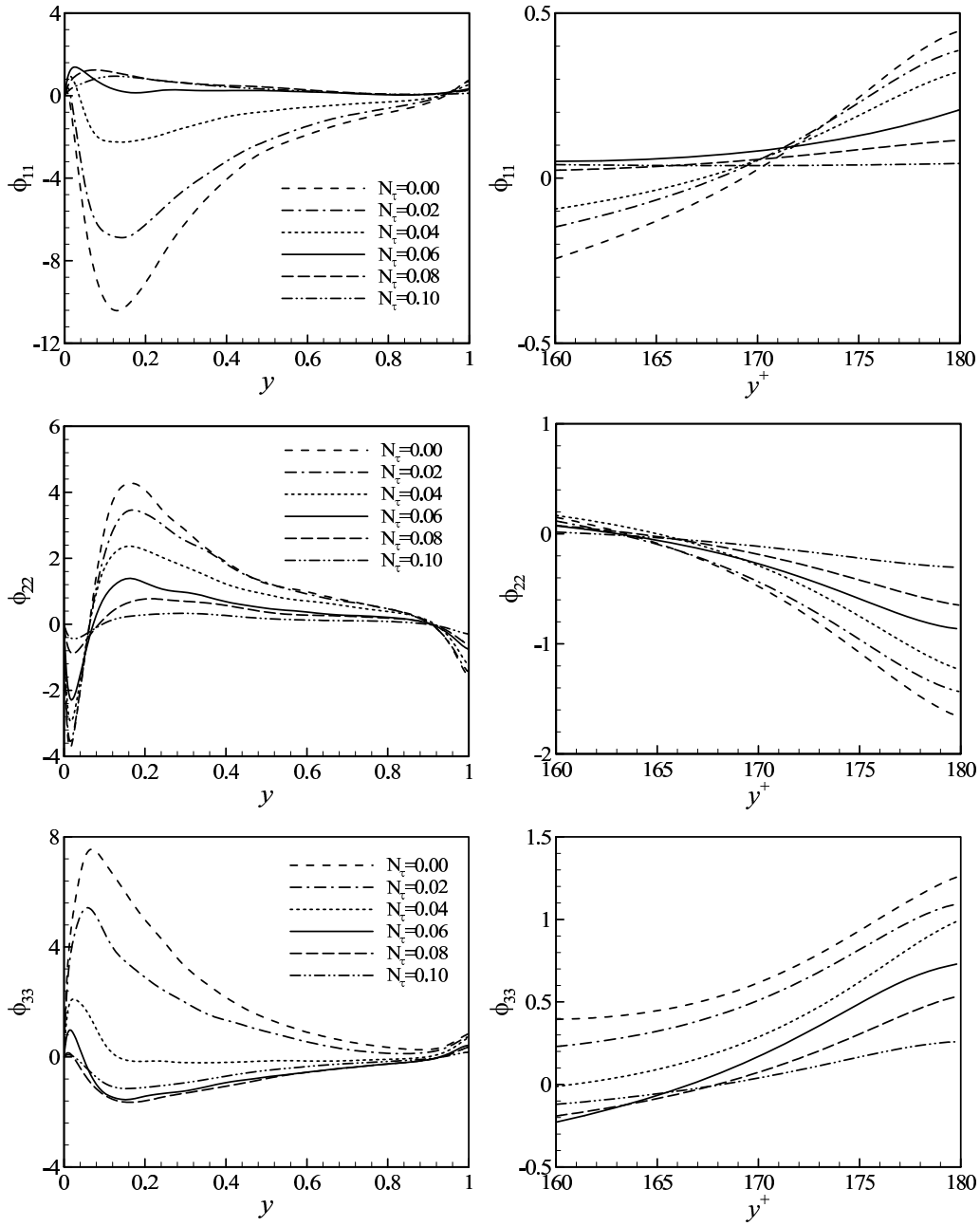

Figure 11: Distributions of the pressure-strain terms in global coordinate (left column) and near the free-surface (right column) in the streamwise, vertical and spanwise directions (from top panels to bottom ones).

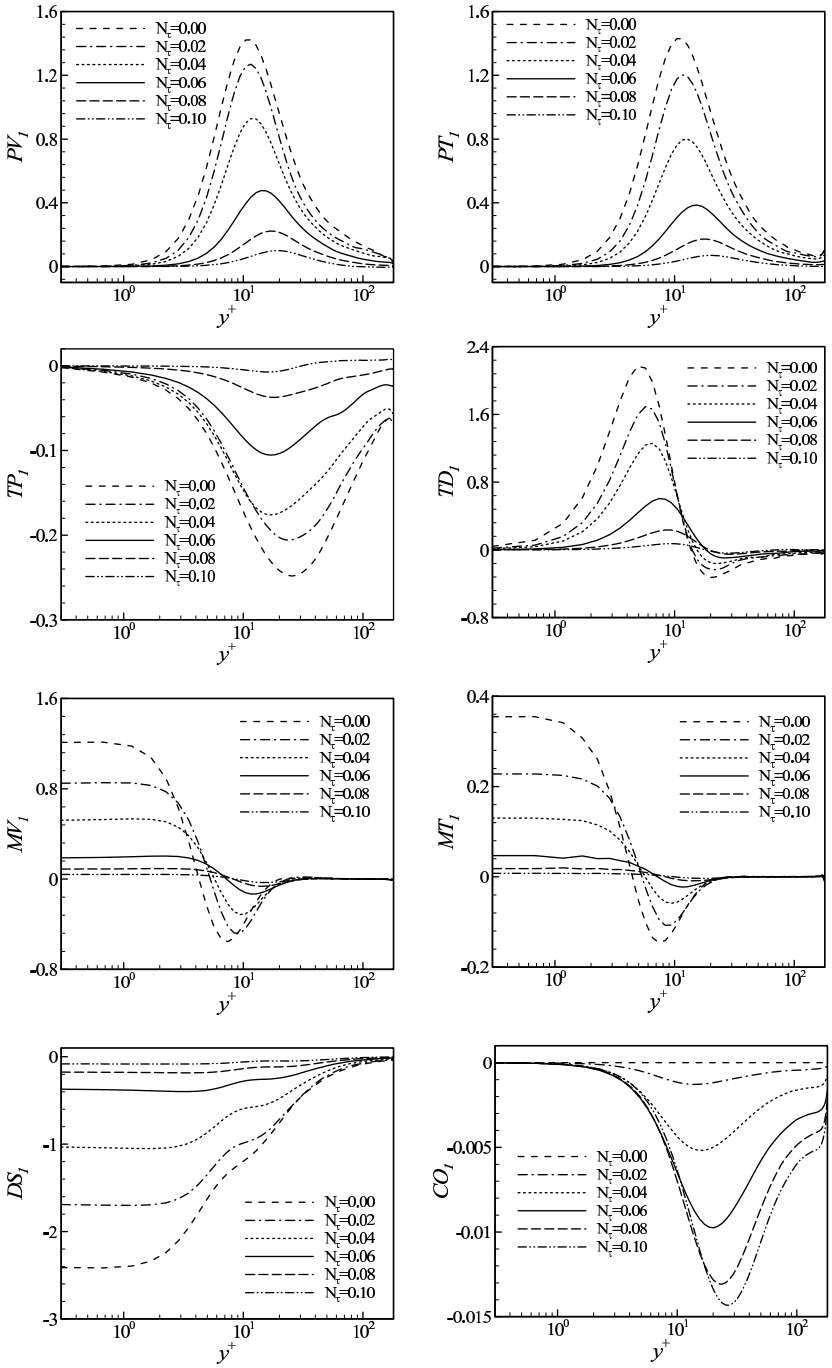

Figure 12: Distributions of the budget terms in the transport equation of $<T'u'>$.

is observed that the magnitudes of these budget terms increase when N_τ varies from 0.02 to 0.06 approximately, and decrease when N_τ varies from 0.06 to 0.1.

Note that, according to Eq. (A.1), the budgets of the streamwise and spanwise turbulent heat fluxes are coupled with each other by the Coriolis force terms, which are represented by $N_\tau < T'w' >$ and $-N_\tau < T'u' >$, respectively. Although the Coriolis force has little influence on the turbulent heat fluxes based on the analysis of the budget terms shown above, it actually plays a significant role in turbulence statistics, which are responsible for thermal statistics.

4.5 Structures of velocity and temperature fluctuations

Structures of the velocity and temperature fluctuations are of great help in revealing the influence of the rotation effect on turbulence coherent structures near the wall and the free surface. Fig. 14 shows the contours of the instantaneous streamwise velocity fluctuation u' in a plane parallel to the wall for $\mathrm{N}_\tau = 0$ and 0.06. Dense elongated near-wall streaky structures in the contour plots of u' occur at $\mathrm{N}_\tau = 0$. As increasing N_τ, e.g., $\mathrm{N}_\tau = 0.06$, the streamwise velocity fluctuation is significantly suppressed with absent streaky structures exhibited in Fig. 14. Near the free surface, the similar behavior is observed. The feature of the streaky structures of the velocity fluctuation is consistent with the turbulence intensities in Fig. 3.

The corresponding instantaneous temperature fluctuation T' fields are shown in Fig. 15. It is identified that the local spots are in accordance with the high- and low-temperature regions alternately. The temperature streaky structures correspond to those of the velocity fluctuations in Fig. 14. These visualizations imply that the turbulent mixing of temperature is controlled by turbulence dynamics.

Due to the effect of rotation, as shown in Figs. 14 and 15, the inclined directions of the structures for the velocity and temperature fluctuations are exhibited obviously. The contours of the velocity and temperature fluctuations demonstrate the alteration of the streamwise and spanwise separations between the streaky structures, compared to the non-rotating flow. Based on the present results (figure not shown), it is found that the streaky structures near the wall and the free surface are nearly in alignment with the local absolute mean flows. The mean spacing and mean inclined angle of the near-wall streaky structures increase obviously with increasing the rotation rate. The behaviors of the near-wall structures are well consistent with those in the wall-normal rotating two-walled channel flows [8].

5 Concluding remarks

Fully developed vertical rotating turbulent open-channel flows with heat transfer have been studied for $N_\tau = 0 - 0.1$, $Re_\tau = 180$ and $\mathrm{Pr} = 1$. The effects of rotation on the characteristics of turbulent flow and heat transfer, in particular in the free surface-influenced layer and in the wall-influenced region, are investigated. Statistical quantities,

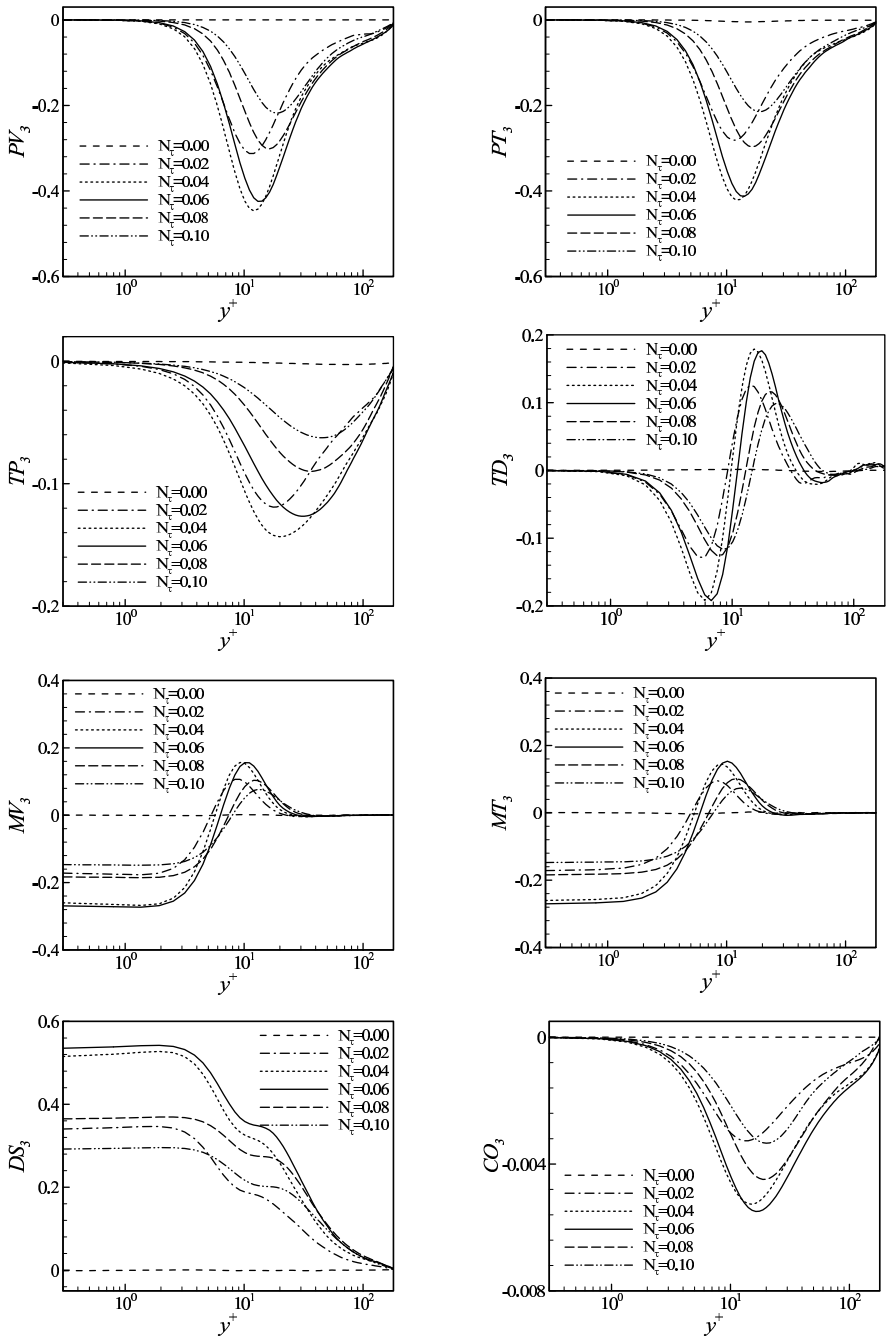

Figure 13: Distributions of the budget terms in the transport equation of $<T'w'>$.

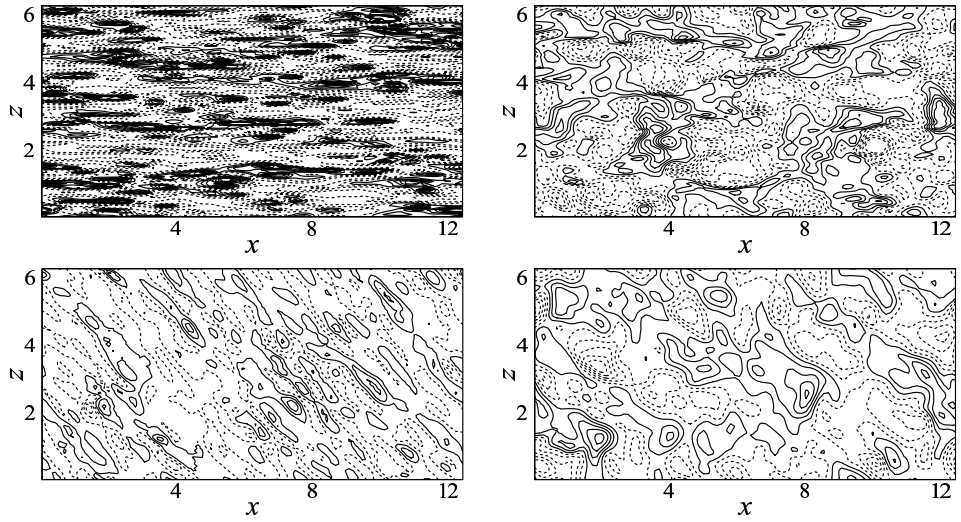

Figure 14: Contours of the instantaneous streamwise velocity fluctuation in a plane parallel to the wall near the wall $y^+ = 2.5$ (left column) and near the free-surface $y^+ = 177.5$ (right column) for $N_\tau = 0$ (upper panels) and 0.06 (lower panels). Here, solid lines represent positive values and dashed lines negative values with increment 0.4.

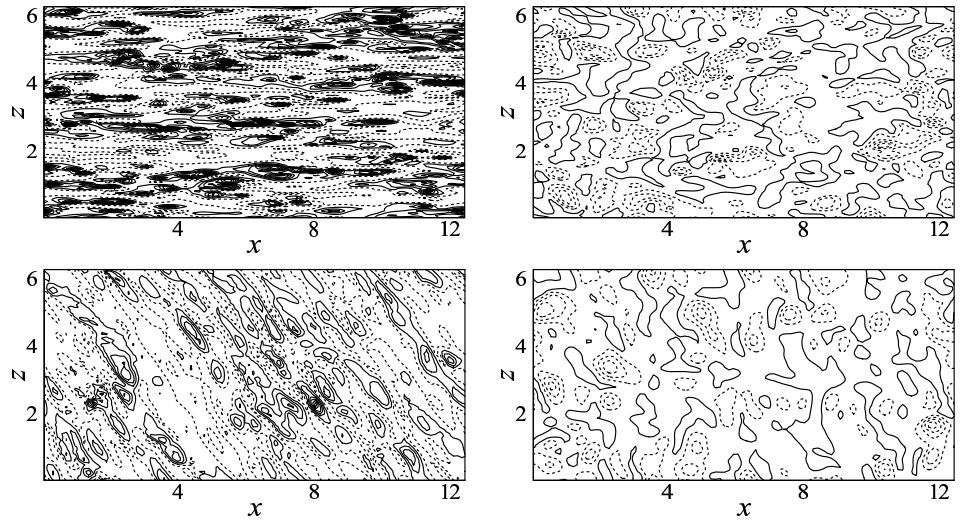

Figure 15: Contours of the instantaneous temperature velocity fluctuation in a plane parallel to the wall near the wall $y^+ = 2.5$ (left column) and near the free-surface $y^+ = 177.5$ (right column) for $N_\tau = 0$ (upper panels) and 0.06 (lower panels). Here, solid lines represent positive values and dashed lines negative values with increment 0.02.

including the mean velocity, temperature and their fluctuations, turbulent heat fluxes, turbulence structures, and the budget terms in the transport equations of Reynolds stresses and turbulent heat fluxes, are analyzed.

The depth of the surface-influenced region can be qualitatively obtained by the position where the free surface begins to dampen the vertical velocity fluctuation, and decreases with increasing the rotation rate. The turbulence intensities have a strong anisotropy near the free surface, which is closely related to anisotropic dissipation and pressure-strain effects. It is revealed that the magnitudes of the pressure-strain terms near the free surface reduce with increasing the rotation rate. In the free surface-influenced layer, the turbulence and thermal statistics are suppressed due to the rotation effect. Thus, the Nusselt number at the free surface decreases as N_τ increases.

In the wall-influenced region, two typical rotation regimes are identified. One is the weak rotation regime with N_τ from 0 to 0.06, and the other is the strong rotation regime with N_τ from 0.06 to 0.1. The streamwise mean velocity $<u>$ decreases monotonically as N_τ increases, indicating that the reduction of wall shear rate is related to the streamwise mean flow. Correspondingly, the spanwise mean velocity $<w>$ increases when N_τ varies from 0 to 0.06 and decreases when N_τ varies from 0.06 to 0.1. When $0 < N_\tau < 0.06$, the statistical quantities correlate with the spanwise velocity fluctuation, e.g., the spanwise turbulence intensity w'_{rms}, the cross stresses $<v'w'>$ and $<u'w'>$, the spanwise turbulent heat transfer $< T'^{+}w' >$, are enhanced since the shear rate of the spanwise mean flow induced by the Coriolis force increases, and the other statistical quantities are suppressed. When $N_\tau > 0.06$, all the turbulence and thermal statistical quantities are suppressed significantly because the effects of rotation play a dominate role in the rotating flows.

Based on the analysis of the Reynolds stress budgets, the turbulence production rate in the streamwise direction becomes weak with increasing rotation rate. However, the turbulence production rate in the spanwise direction increases significantly when $0 < N_\tau < 0.06$ and obviously decreases when $N_\tau > 0.06$. In the analysis of the budget terms in the transport equations of turbulent heat fluxes, although the Coriolis force has little influence on the turbulent heat fluxes, it actually plays a significant role in turbulence statistics, which is closely related to the characteristics of turbulent heat transfer. The magnitudes of the budget terms in the transport equation of spanwise turbulent heat flux increase when N_τ varies from 0.02 to 0.06 approximately and decrease when N_τ varies from 0.06 to 0.1.

The streaky structures based on the velocity and temperature fluctuations near the wall and the free surface are nearly in alignment with the local absolute mean flows. The mean spacing and mean inclined angle of the near-wall streaky structures increase obviously with the increase of the rotation rate. The temperature streaky structures are consistent with those of the velocity fluctuations. These structures imply that the turbulent mixing of temperature is controlled by turbulence dynamics.

Acknowledgements

This work was supported by the National Natural Science Foundation of China (Nos. 90405007, 10302028, 10125210), the Hundred Talents Program of the Chinese Academy of

Sciences, and Specialized Research Fund for the Doctoral Program of Higher Education (No. 20020358013). The authors thank referees for valuable comments.

Appendix: Equations for Turbulent Heat Fluxes

The transport equation for the turbulent heat fluxes $< T'u_i' >$ in the vertical rotating channel flow can be written as

$$\begin{aligned} & \frac{\partial < T'u_i' >}{\partial t} + < u_j > \frac{\partial < T'u_i' >}{\partial x_j} \\ = \; & PV_i + PT_i + TP_i + TD_i + MV_i + MT_i + DS_i + CO_i \end{aligned} \tag{A.1}$$

where the terms on the right-hand side are expressed as

$PV_i = - < u_j'T' > \partial < u_i > /\partial x_j$	production rate by mean velocity gradient;
$PT_i = - < u_i'u_j' > \partial < T > /\partial x_j$	production rate by mean temperature gradient;
$TP_i = - < T'(\partial p'/\partial x_i) >$	temperature pressure gradient correlation;
$TD_i = -\partial < u_i'u_j'T' > /\partial x_j$	turbulent diffusion;
$MV_i = 1/Re_\tau < \partial/\partial x_j[T'(\partial u_i'/\partial x_j)] >$	molecular diffusion relevant to velocity fluctuation;
$MT_i = 1/(Re_\tau \Pr) < \partial/\partial x_j[u_i'(\partial T'/\partial x_j)] >$	molecular diffusion relevant to temperature fluctuation;
$DS_i = -[1/Re_\tau + 1/(Re_\tau \Pr)] < (\partial u_i'/\partial x_j)(\partial T'/\partial x_j) >$	dissipation rate;
$CO_i = -\varepsilon_{ijk} N_\tau (\Omega_j/\lvert\Omega\rvert) < u_k'T' >$	Coriolis force term.

Nomenclature

h	height of the channel	k	thermal conductivity
Nu	Nusselt number	N_τ	rotation number
p	effective pressure	Pr	Prandtl number
q_F	mean heat flux at the free surface	Re_τ	Reynolds number based on the friction velocity
t	time	T	temperature
T_F	temperature at the free surface	T_W	temperature at the wall
T_τ	friction temperature	T'	temperature fluctuation
u	streamwise velocity	u'	streamwise velocity fluctuation
u_i	velocity component in the i-direction	u_i'	velocity fluctuation in the i-direction

u_τ	friction velocity	v	vertical velocity
v'	vertical velocity fluctuation	w	spanwise velocity
w'	spanwise velocity fluctuation	x	streamwise coordinate
x_i	Cartesian coordinate axes	y	vertical coordinate
y^+	vertical distance from the wall normalized by the friction velocity	y_D^+	depth of the surface-influenced region
z	spanwise coordinate	ν	molecular kinematic viscosity
κ	thermal diffusivity	ρ	fluid density
ϕ_{ij}	pressure-strain tensor	Ω	angular velocity of system rotation
$<>$	average in time and in the plane parallel to the wall		

Subscripts: rms root mean square
Superscripts: + normalized quantity by wall parameters

References

[1] H. B. Wu and N. Kasagi, Effects of arbitrary directional system rotation on turbulent channel flow, Phys. Fluids, 16 (2004), 979-990.
[2] J. P. Johnston, R. M. Halleen and D. K. Leziius, Effects of spanwise rotation on the structure of two-dimensional fully developed turbulent channel flow, J. Fluid Mech., 56 (1972), 533-557.
[3] R. Kristoffersen and H. I. Andersson, Direct simulations of low-Reynolds number turbulent flow in a rotating channel, J. Fluid Mech., 235 (1993), 163-197.
[4] U. Piomelli and J. Liu, Large-eddy simulation of rotating channel flows using a localized dynamic model, Phys. Fluids, 7 (1995), 839-848.
[5] K. Nakabayashi and O. Kitoh, Low Reynolds number fully developed turbulent channel flow with system rotation, J. Fluid Mech., 315 (1996), 1-29.
[6] E. Lamballais, O. Metais and M. Leiseur, Spectral-dynamical model for large-eddy simulations of turbulent rotating channel flow, Theor. Comp. Fluid Dyn., 12 (1998), 149-177.
[7] Y. Nagano and H. Hattori, Direct numerical simulation and modelling of spanwise rotating channel flow with heat transfer, J. Turbul., 4 (2003), 10.
[8] B. Y. Li, N. S. Liu and X. Y. Lu, Direct numerical simulation of wall-normal rotating turbulent channel flow with heat transfer, Int. J. Heat Mass Tran., in press.
[9] I. Esau, The Coriolis effect on coherent structures in planetary boundary layers, J. Turbul., 4 (2003), 17.
[10] C. G. Speziale, B. A. Younis, R. Rubinstein and Y. Zhou, On consistency condition for rotating turbulent flows, Phys. Fluids, 22 (1998), 2108-2110.
[11] Y. Nagano and H. Hattori, An improved turbulence model for rotating shear flows, J. Turbul., 3 (2002), 6.
[12] H. Kawamura, K. Ohsaka, H. Abe and K. Yamamoto, DNS of turbulent heat transfer in channel flow with low to medium-high Prandtl number fluid, Int. J. Heat Fluid Flow, 19 (1998), 482-491.
[13] H. Kawamura, H. Abe and Y. Matsuo, DNS of turbulent heat transfer in channel flow with respect to Reynolds and Prandtl number effects, Int. J. Heat Fluid Flow, 20 (1999), 196-207.
[14] R. Verzicco and P., Orlandi, A finite difference scheme for direction simulation in cylindrical coordinates, J. Comput. Phys., 123 (1996), 402-414.

[15] J. Kim and P. Moin, Application of a fractional-step method to incompressible Navier-Stokes equations, J. Comput. Phys., 59 (1985), 308-323.
[16] M. M. Rai and P. Moin, Direct simulations of turbulent flow using finite-difference schemes, J. Comput. Phys., 96 (1991), 15-53.
[17] J. Kim, P. Moin and R. Moser, Turbulence statistics in fully developed channel flow at low Reynolds number, J. Fluid Mech., 177 (1987), 133-166.
[18] P. Orlandi, Helicity fluctuations and turbulent energy production in rotating and non-rotating pipes, Phys. Fluids, 9 (1997), 2045-2056.
[19] P. Orlandi and D. Ebstein, Turbulent budgets in rotating pipes by DNS, Int. J. Heat Fluid Flow, 21 (2000), 499-505.
[20] P. Orlandi and M. Fatica, Direct simulations of turbulent low in a pipe rotating about its axis, J. Fluid Mech., 343 (1997), 43-72.
[21] Y. K. Pan, T. Tanaka and Y. Tsuji, Direct numerical simulation of particle-laden rotating turbulent channel flow, Phys. Fluids, 13 (2001), 2320-2337.
[22] S. Y. Chung, G. H. Rhee and H. J. Sung, Direct numerical simulation of turbulent concentric annular pipe flow Part 1: Flow field, Int. J. Heat Fluid Flow, 23 (2002), 426-440.
[23] G. Vittor and R. Verzicco, Direct simulation of transition in an oscillatory boundary layer, J. Fluid Mech., 371 (1998), 207-232.
[24] M. Quadrio and S. Sibilla, Numerical simulation of turbulent flow in a pipe oscillating around its axis, J. Fluid Mech., 424 (2000), 217-241.
[25] S. Grossmann and D. Lohse, On geometry effects in Rayleigh-Bénard convection, J. Fluid Mech., 486 (2003), 105-114.
[26] N. S. Liu and X. Y. Lu, Large eddy simulation of turbulent concentric annular channel flows, Int. J. Numer. Methods Fluids, 45 (2004), 1317-1338.
[27] Y. H. Dong and X. Y. Lu, Large eddy simulation of a thermally stratified turbulent channel flow with temperature oscillation on the wall, Int. J. Heat Mass Tran., 47 (2004), 2109-2122.
[28] L. Wang and X. Y. Lu, An investigation of turbulent oscillatory heat transfer in channel flows by large eddy simulation, Int. J. Heat Mass Tran., 47 (2004), 2161-2172.
[29] L. Wang, Y. H. Dong and X. Y. Lu, An investigation of turbulent open channel flow with heat transfer by large eddy simulation, Comput. Fluids, 34 (2005), 23-47.
[30] X. Y. Lu, S. W. Wang, H. G. Sung, S. Y. Hsieh and V. Yang, Large eddy simulations of turbulent swirling flows injected into a dump chamber, J. Fluid Mech., 527 (2005), 171-195.
[31] L. Wang and X. Y. Lu, Large eddy simulation of stably stratified turbulent open channel flows with low- to high-Prandtl number, Int. J. Heat Mass Tran., 48 (2005), 1883-1897.
[32] N. S. Liu and X. Y. Lu, Large eddy simulation of turbulent flows in a rotating concentric annular channel, Int. J. Heat Fluid Flow, 26 (2005), 378-392.
[33] Y. H. Dong and X. Y. Lu, Direct numerical simulation of stably and unstably stratified open channel flows, Acta Mech., 177 (2005), 115-136.
[34] P. Moin and J. Kim, Numerical investigation of turbulent channel flow, J. Fluid Mech., 118 (1982), 341-377.
[35] I. Calmet and J. Magnaudet, Statistical structure of high-Reynolds-number turbulence close to the free surface of an open-channel flow, J. Fluid Mech., 474 (2003), 355-378.
[36] L. Y. Zou, N. S. Liu and X. Y. Lu, An investigation of pulsating turbulent open channel flow by large eddy simulation, Comput. Fluids, 35 (2006), 74-102.
[37] H. Tennekes and J. L. Lumley, A First Course in Turbulence, MIT Press, Cambridge, MA, 1972, pp. 95-97.
[38] Y. H. Dong, X. Y. Lu and L. X. Zhuang, Large eddy simulation of turbulent channel flow

with mass transfer at high-Schmidt numbers, Int. J. Heat Mass Tran., 46 (2003), 1529-1539.
[39] S. Komori, Y. Murakami and H. Ueda, The relationship between surface-renewal and bursting motions in an open-channel, J. Fluid Mech., 203 (1989), 103-123.
[40] M. Rashidi, G. Hetstroni and B. Banerjee, Mechanisms of heat and mass transport at gas-liquid interfaces, Int. J. Heat Mass Tran., 34 (1991), 1799-1805.
[41] C. N. S. Law and B. C. Khoo, Transport across a turbulent air-water interface. AIChE J., 48 (2002), 1856-1968.
[42] N. N. Mansour, J. Kim and P. Moin, Reynolds-stress and dissipation-rate budgets in a turbulent channel flow, J. Fluid Mech., 194 (1988), 15-44.
[43] B. Perot and P. Moin, Shear-free boundary layers: 1. Physical insights into near wall turbulence, J. Fluid Mech., 295 (1995), 199-227.